THE JOURNAL OF PHYSICAL CHEMISTRY Letters

Cite This: J. Phys. Chem. Lett. 2018, 9, 2546−2553

Letter

pubs.acs.org/JPCL

Anomalous Nanoscale Optoacoustic Phonon Mixing in Nematic Mesogens

Dima Bolmatov,[*,†,‡] Dmytro Soloviov,[§,∥,⊥] Dmitry Zav'yalov,[#] Lewis Sharpnack,[▽] Deña M. Agra-Kooijman,[○] Satyendra Kumar,[◆] Jiawei Zhang,[¶] Mengkun Liu,[¶] and John Katsaras[†,‡]

[†]Neutron Scattering Directorate, Oak Ridge National Laboratory, Oak Ridge, Tennessee 37831, United States

[‡]Department of Physics and Astronomy, University of Tennessee, Knoxville, Tennessee 37996, United States

[§]Frank Laboratory of Neutron Physics, Joint Institute for Nuclear Research, Dubna 141980, Russia

[∥]Taras Shevchenko National University of Kyiv, Kyiv 01033, Ukraine

[⊥]Moscow Institute of Physics and Technology, Dolgoprudny 141701, Russia

[#]Volgograd State Technical University, Volgograd 400005, Russia

[▽]European Synchrotron Radiation Facility, Grenoble 38043, France

[○]Liquid Crystal Institute, Kent State University, Kent, Ohio 44242, United States

[◆]Division of Research and Department of Physics, University at Albany, Albany, New York 12222, United States

[¶]Department of Physics and Astronomy, Stony Brook University, Stony Brook, New York 11794, United States

ABSTRACT: Recent inelastic X-ray scattering (IXS) experiments on mesogens have revealed entirely new capabilities with regards to their nanoscale phonon-assisted heat management. Mesogens such as nematic liquid crystals (LCs) are appealing systems for study because their structure and morphology can easily be tuned. We report on *Q*-resolved ultra-high-resolution IXS, X-ray diffraction, and THz time-domain spectroscopy experiments combined with large-scale all-atom molecular dynamics simulations on the dynamic properties of 5CB LCs. For the first time, we observe a strong mixing of phonon excitations originating from independent in-phase and out-of-phase van-der-Waals-mediated displacement patterns. The coexistence of transverse acoustic and optical modes of 5CB LCs at near room temperature is revealed through the emergent transverse phonon gap and THz light−phonon coupling taking place within the same energy range. Furthermore, our experimental observations are supported by analysis showing correlations of spontaneous fluctuations of LCs on picosecond time scales. These findings are significant for the design of a new generation of soft molecular vibration-sensitive nanoacoustic and optomechanical applications.

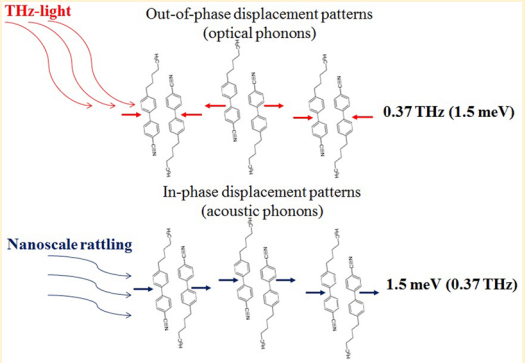

A landmark in the history of electro-optical displays marked in 1973 with the discovery of 4-cyano-4′-pentylbiphenyl (5CB),[1] a nematic liquid crystal (LC) and the first of the cyanobiphenyls. Since then, these systems have been extensively studied mainly as they pertain to display-related technologies.[2−7] In doing so, however, other fascinating phenomena involving quasiparticles as phonons have barely been explored in these materials. Phonons are mechanical vibrations that exist in the form of sound and heat occurring at different frequency and length scales.[8−11] The first operates at relatively low and intermediate frequencies, and is able to travel over long distances, while the latter appears at elevated frequencies propagating at the meso- and nanoscale. Sound propagation and heat transfer have been well researched in conventional materials. However, these phenomena currently represent scientific and technological challenges when it comes to exotic materials such as phononic crystals (PnCs).[12] PnCs are complex materials with artificially engineered architectures created to generate dynamic responses to specific phonon excitations beyond those available in naturally occurring materials.[13,14] PnCs are capable of creating zones forbiding the propagation of vibrational waves, known as phononic gaps, which provide exceptional possibilities with regards to sound manipulation and heat management.[15,16] Such materials can be used as metamaterials, including but not limited to, sonic cloaking,[17] acoustic diodes,[18] ultrasound mirrors,[19] hypersound crystals,[20] thermoelectrics,[21] and THz optomechanical metamaterials[22,23] covering the entire phonon spectrum from sound (kHz) up to heat (THz). Nanoscale heat management and energy transfer at THz frequencies has recently attracted much attention.[24−28] Nevertheless, the main efforts expended to harnessing the THz molecular vibrations have primarily been

Received: March 26, 2018
Accepted: April 28, 2018
Published: April 29, 2018

DOI: 10.1021/acs.jpclett.8b00926
J. Phys. Chem. Lett. 2018, 9, 2546−2553

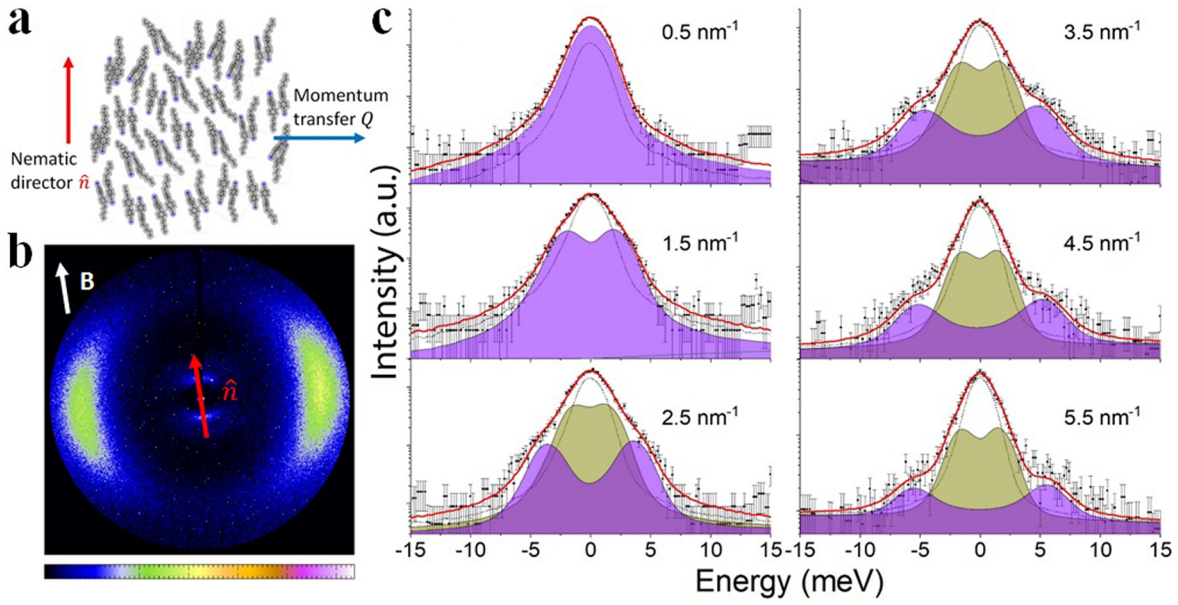

Figure 1. Phonon excitations and structure in the nematic phase. (a) Schematic of the IXS scattering geometry of 5CB LC at T = 28 °C. The scattering plane is orthogonal to the figure plane. (b) 5CB X-ray diffraction pattern. White and red arrows denote the direction of the applied magnetic field B and the nematic director $\hat{\mathbf{n}}$, respectively. (c) IXS spectra of the 5CB sample. The measured experimental scans (black squares) are presented together with the error bars, the corresponding Q values, the resolution function (black dotted line), and the best fitting curve (red solid line) composed of two damped harmonic oscillator (DHO) excitations: purple and olive solid lines with the filled areas below them, respectively.

focused on the utilization of rigid-based materials,[29−31] despite recent discoveries showing solid-like dynamic responses in soft materials.[32−36] In this regard, further explorations of soft matter THz vibrational landscapes are needed because their morphological and structural properties can be controlled and manipulated. Moreover, such studies may pave the way to a new class of PnCs on nanometer−terahertz scales based on structurally tuned soft materials.

Here we report on the first observation of the opto-acoustic phonon mixing effect in thermotropic mesogens using Q-resolved inelastic X-ray scattering (IXS), X-ray diffraction (XRD), and THz time-domain spectroscopy (TDS) experiments combined with large-scale all-atom molecular dynamics (MD) simulations. IXS measurements enabled us to determine two independent phonon branches. Importantly, the IXS data contain clear features of the transverse phonon gap in the low-Q regime, pointing to the transverse acoustic nature of the phonon gap. In contrast, analysis of the correlations of spontaneous fluctuations, based on calculations of the velocity−velocity correlation functions (VCFs), indicates the existence of out-of-phase displacement patterns operating on the same characteristic energy−time scales. This implies the emergence of the optical phonon mode coexisting with the acoustic mode. Finally, the MD-based correlation functions analysis is supported by the THz TDS observation of a sharp absorption of THz light.

The IXS scattering geometry and diffraction pattern from a thermotropic 5CB sample in the nematic phase (T = 28 °C) is shown in Figure 1a,b, respectively. Thermotropic LCs in the nematic phase are characterized by mesogens that have no positional order but tend to align in the same direction; they are also sensitive to changes in temperature. The orientation of the mesogens is based on the director $\hat{\mathbf{n}}$ (see Figure 1a). The XRD data were obtained from a 5CB sample (Sigma-Aldrich, 98% purity) taken up into a 1 mm diameter quartz capillary (Charles Supper) that was flame-sealed. The measurements were performed using the sample environment and diffractometer previously described.[37] The arcs at wide angle, centered at Q = 14.07 nm^{-1} with a full width at half-maximum (fwhm) 4.83 nm^{-1}, correspond to an effective molecular width of 0.45 nm and a correlation length of 1.30 nm. This indicates that the mesogens are only sensitive to positions up to their third nearest neighbors. The arcs at small angle, centered at Q = 2.55 nm^{-1} with the fwhm of 1.12 nm^{-1}, correspond to an effective length of 2.46 nm and a correlation length of 5.60 nm, indicating short-range order. The effective length at small angle is 1.4 times the molecular length of the 5CB molecule (1.8 nm), consistent with antiparallel alignment of the cyanobiphenyl cores of neighboring molecules.[37] In Figure 1c, we present IXS measurements with unprecedented spectral contrast,[38] making it possible to detect phonon excitations down to the extremely low Q value of 0.5 nm^{-1}. To study 5CB samples with IXS, a cell was constructed from borosilicate glass slides of dimensions 2 × 25 mm. The plates were then treated with Quilon H to generate homeotropic alignment. After this treatment, the plates were separated by 200 μm thick Teflon spacers, fixed with epoxy, and filled with 5CB (Sigma-Aldrich). The temperature during measurements was controlled using a Linkam LTS420 hot stage. The high spectral contrast of the resolution function (black dotted line) with a nearly Gaussian line shape was key for determining phonon features in the framework of the damped harmonic oscillator (DHO) model.[35] The IXS energy scans (see Figure 1c) were measured between 0.5 and 5.5 nm^{-1} at 1 nm^{-1} increments. The change in the central peak slope led to the emergence of a transverse mode in the IXS spectrum at a Q value of 2.5 nm^{-1} (Q_{gap} value, Figure 1c), whereas the more energetic longitudinal acoustic (LA) mode started at Q = 0.5 nm^{-1}. Importantly, the average distance between mesogens is 0.45 nm, and they are only sensitive to adjacent molecules up to third nearest neighbor (XRD data). This means that the size of a rattling domain consists of six mesogens in its diameter, which is approximately

DOI: 10.1021/acs.jpclett.8b00926
J. Phys. Chem. Lett. 2018, 9, 2546−2553

two times larger than the correlation length (1.3 nm). If the 5CB mesogen was flat, then they could Pi-Pi stack, which would place them closer to 0.33 nm apart, but because there is a twist between the two carbon rings in the CB, they tend to sit a little further apart. The molecules also have a great deal of rotational freedom in the nematic phase, and hence this also contributes to the increased distance. Therefore, the size of a picosecond-time-scale-lived rattling domain d is 2.7 nm, giving rise to an estimated phonon gap value in reciprocal space of 2.33 nm^{-1} ($Q_{gap} = \frac{2\pi}{d}$), in good agreement with IXS data (Q_{gap} = 2.5 nm^{-1}). Therefore, the shear restoring forces become negligible in sustaining the propagation of transverse vibrations beyond a distance of 2.7 nm, implying that transverse phonons cannot be excited below 2.33 nm^{-1} (XRD data). This limits the threshold of the Q_{gap} at a value of 2.5 nm^{-1} (IXS data). Nevertheless, the determination of a precise Q_{gap} value via IXS requires higher spectral resolution using finer Q-value increments, as compared to our present measurements (1 nm^{-1} Q-value increments).

The dynamic behavior of the transverse branch contains features from both conventional transverse acoustic (TA) and transverse optical (TO) modes (see Figure 2), both common in the phonon landscapes of soft materials.[36] On the one hand, the emergence of a phonon gap in the TA-TO mode coexistence is the fingerprint of TA excitations previously observed in partially disordered systems, such as biological membranes,[35] LCs,[36] and classical liquids.[39] The heat and energy transfer in such systems is primarily accomplished due to local short-lived (picosecond time scale), in-phase rattling events (see Figure 2b). Restoring shear forces become negligible at long- and intermediate-range order in real space due to elevated anharmonic effects,[40] which is reflected in the overdamping dynamic character of the low-Q phonon excitations in reciprocal space, resulting in the emergence of the acoustic phonon gap.[41] On the other hand, the weakly dispersive phonon behavior of this mode (see Figure 2a), and the previous observation of breathing modes (standing waves) in cyanobiphenyl LCs via ultralow Raman measurements within 1.2 to 2.4 meV (0.29−0.58 THz),[42] indicate the mode's optical nature which originates from out-of-phase van-der-Waals-mediated displacement patterns (see Figure 2b).

To gain some insight into the origins of this mode, we ran large-scale atomistic MD simulations using the CHARMM27 force field.[43] This force field contains energetics and electrostatics of intermolecular harmonic potentials of stretching, bending, torsion, and van der Waals potentials, including Coulomb terms.[44] The simulated 5CB system consisted of 8000 mesogens, or 152 000 atoms, and the MD simulations were ran using the LAMPPS package. First, the simulated system was energetically optimized and thermally equilibrated (thermalization stage) in the NVT ensemble (pressure = 1 atm, temperature = 28 °C, density = 1.02 g/cm^3). Then, thermalization was done using the Berendsen thermostat over 400 ps with 1 fs steps. In the production stage, the system was confined in the NPT ensemble, employing the Nosé−Hoover thermostat with the Parrinello−Rahman algorithm as the barostat. This simulation was run for 1 ns in 1 fs increments. Furthermore, we calculated the time-dependent correlation functions. Specifically, the analysis is based on velocity−velocity autocorrelation functions (VACFs) and cross velocity−velocity correlation function (VCF), which are capable of revealing the nature of the phonon excitations.

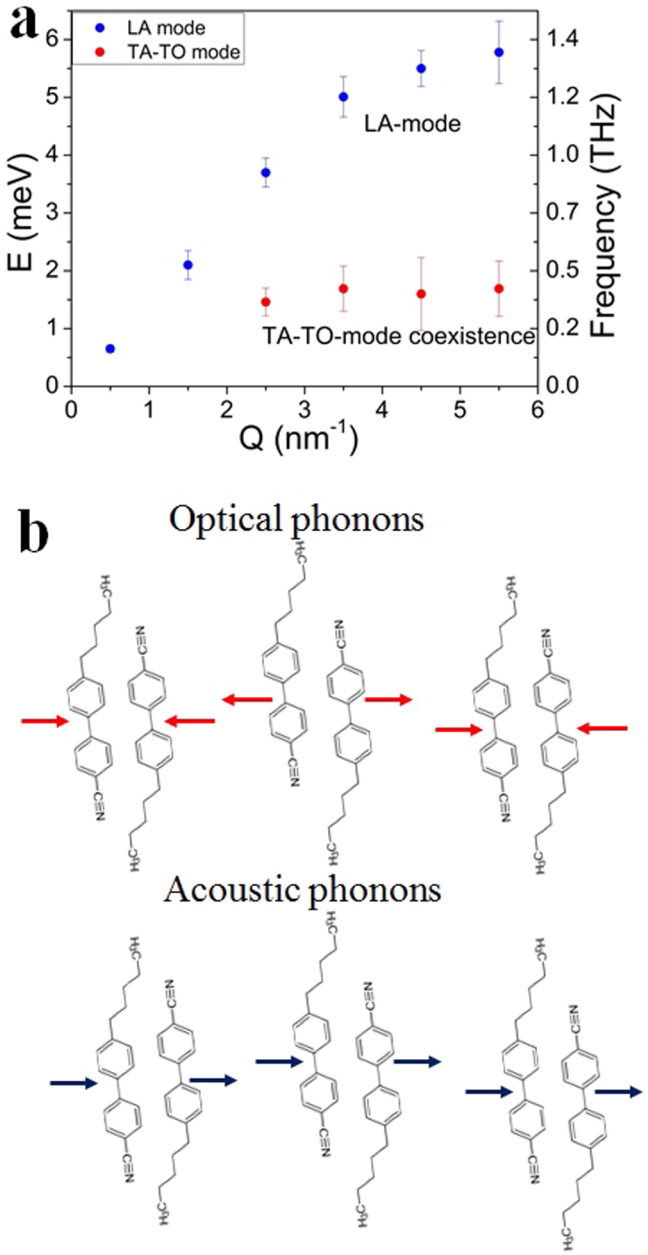

Figure 2. (a) 5CB phonon dispersions of LA and TA-TO modes measured by IXS. The estimated longitudinal sound velocity is ∼2680 m/s. (b) Schematic representation of out-of-phase (TO mode) and in-phase (TA mode) displacement patterns in nematic mesogens.

Green and Kubo introduced the so-called transport coefficients as integrals over a time-correlation function in thermal equilibrium.[45,46] In the framework of the Green−Kubo formalism, it was demonstrated that a system relaxes toward equilibrium whenever it is taken out of its equilibrium state by an external force. At the same time, the dissipation of fluctuations has exactly the same physical origin[45,46] but has yet to be observed. 5CB is composed of two phenyl rings (biphenyl) terminated by a CN (cyano) group at one end and an alkyl chain (pentyl) at the other (see the inset in Figure 3a). Here we calculate VACFs over centers of mass of alkyl tails and biphenyls, and VCF across alkyl tail−biphenyl centers of mass. The normalized velocity correlation function $\Psi_{a,b}(t)$ can be presented in its general form as:

DOI: 10.1021/acs.jpclett.8b00926
J. Phys. Chem. Lett. 2018, 9, 2546−2553

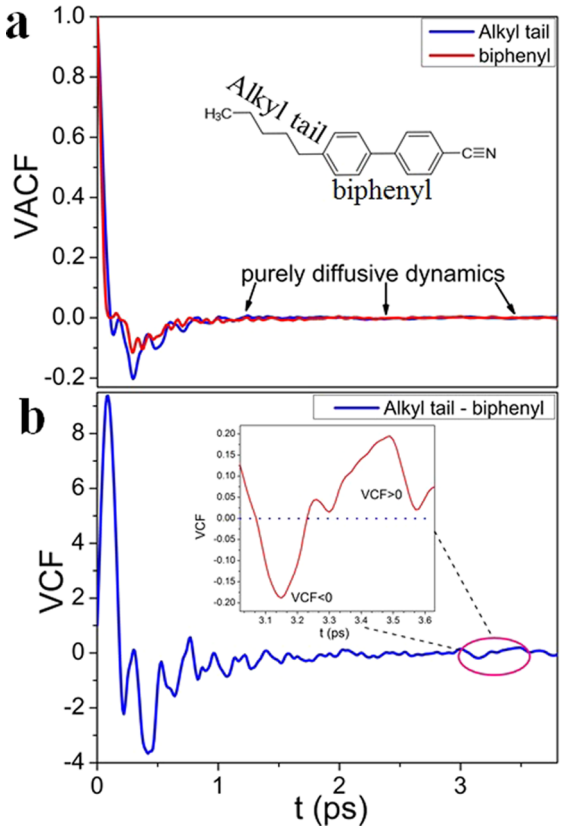

Figure 3. Velocity correlation functions of nematic 5CB LCs: (a) VACF of alkyl tails and biphenyls and (b) VCF of alkyl tail−biphenyl centers of mass.

$$\Psi_{a,b}(t) = \frac{<\vec{\mathbf{v}}_a(t_0)\cdot\vec{\mathbf{v}}_b(t_0+t)>}{<\vec{\mathbf{v}}_a(t_0)\cdot\vec{\mathbf{v}}_b(t_0)>} \quad (1)$$

where $\vec{\mathbf{v}}(t)$ is the velocity vector and < > denotes a time average over all ensembles and t_0. When $a = b$, it corresponds to VACF; otherwise, it corresponds to VCF. The rapid decrease in VACFs (see Figure 3a) up to 0.5 ps implies a decrease in the pair correlations of both alkyl tail and biphenyl motions along the trajectories of their centers of mass. Beyond 1 ps, VACFs instantly become shallow, indicative of a purely diffusive dynamic behavior. However, the VCF across alkyl tail−biphenyl centers of mass exhibits oscillatory behavior (in-phase rattling patterns) over short and intermediate times as a consequence of the strong dipole−dipole interaction[47] between antiparallelly aligned 5CB molecules (see Figure 1a). Remarkably, at about 3.1 to 3.2 ps (0.32 THz, 1.4 meV) the VCF undergoes a dip (VCF < 0, see Figure 3b), quickly evolving into a nondiffusive regime (VCF ≠ 0) lasting up to 3.5 ps and exhibiting correlations of spontaneous fluctuations (Onsager's regression hypothesis[48]). This implies that alkyl tail−biphenyl centers of mass experience alkyl tail−biphenyl collisions at ∼3.1 ps, meaning that adjacent tails and biphenyl cores move in opposite directions after a collision event. Therefore, the neighboring tails and cores locally form out-of-phase displacement patterns over 3.1 to 3.2 ps across the entire 5CB system. A nondiffusive behavior (VCF ≠ 0) from 3.1 up to 3.5 ps, combined with the nonoscillatory motions of tails and cores, without any collisions (localization,[49] VCF > 0 consistently), indicates their nonpropagating dynamic character, commonly known as breathing modes (standing waves, optical phonons).

The existence of nonpropagating breathing modes (optical phonons) originating from out-of-phase displacement patterns implies their ability to interact with light at corresponding energies/frequencies. THz TDS is a very powerful technique used to carry out vibrational spectroscopy at frequencies spanning from 0.2 THz up to 15 THz.[50,51] Spectroscopy into the properties of organic molecules has been a field of particular importance because the low-photon energy at THz frequencies makes it possible to excite intermolecular motions utilizing THz TDS. Here we present measurements on 5CB LCs using the experimental capabilities of the THz TDS technique to probe optical phonons due to THz light−phonon coupling. The 5CB sample used for THz TDS measurements was held between 2 × 25 mm glass plates separated by a 1 mm glass spacer and fixed by fusing the glass plates. Because of the amounts of sample required by the THz TDS technique (several hundred by several hundred micrometers) and the resultant sample thickness, it was not possible to align the molecules using only surface anchoring; instead, a magnetic field was needed to generate the alignment. Specifically, two magnets were used to generate a vertical magnetic field in the alignment, perpendicular to the THz electric field polarization. The THz pulse (see Figure 4a) was generated by sending ultrafast light pulses (1.3 W, 800 nm, 35 fs, and 1 kHz repetition rate) through a ZnTe crystal. Because of the optical nonlinearity of ZnTe, a varying nonlinear polarization, P, is induced and follows the intensity envelop of the 35 fs pulse. The varying polarization P then acts as a THz source whose electric-field profile is proportional to the second derivative of P (see Figure 4b, blue curve). The resultant transmission beam as a result of placing the sample at the focus of the generated THz beam is represented by the green curve (see Figure 4b). The transmission of the THz light from the 5CB sample was measured between 0.2 and 0.8 THz using air as the reference (see Figure 4b). Furthermore, a Fast Fourier Transform (FFT) was used, converting the THz pulses from the time to the frequency domain (see Figure 4c). In doing so, we detected the absorption dips in the transmission profile at 0.26 (1.1 meV), 0.37 (1.5 meV), and 0.51 THz (2.1 meV), respectively (see Figure 4c). The detection of the absorption dip at 0.37 THz (1.5 meV) is of particular significance because it is in good agreement with the IXS data (see Figure 2a), the MD-based VCF analysis (see Figure 3b), and the ultralow Raman[42] and ultrabroadband THz spectroscopy measurements.[52] This compelling evidence of the opto-acoustic phonon mixing effect in nematic mesogens stems from the detection of the emergent phonon gap (nature of acoustic phonons) via IXS experiments and the sharp light absorption in the THz TDS measurements (nature of optical phonons).

Importantly, the concept of an acoustic transverse phonon gap in soft (noncrystalline) materials can be readily understood by simple physical considerations of relaxation processes and characteristic vibrational energies, in contrast with their solid-state counterparts. In solid-state materials, mechanical vibrations can propagate over relatively long distances, implying the existence of vibrational modes at very low frequencies. In soft materials, because of nonlinear anharmonic effects, vibrations get damped at the intermediate or long-range scales, leading to the disappearance of low-frequency excitations. Specifically, a phonon frequency of a soft material can be represented as $\omega = \frac{2\pi}{\tau}$, where τ is the relaxation time. Using

DOI: 10.1021/acs.jpclett.8b00926
J. Phys. Chem. Lett. 2018, 9, 2546−2553

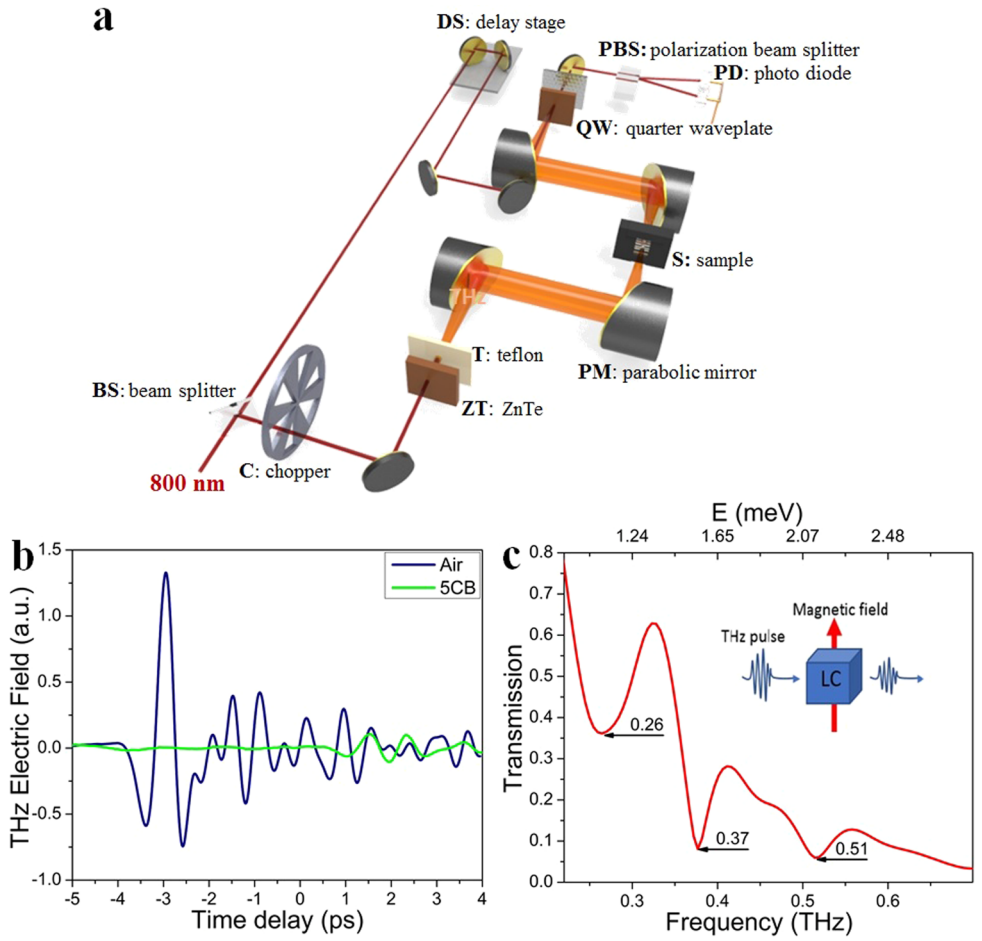

Figure 4. (a) Schematic of the THz TDS experimental setup. (b) Transmitted THz electric field profiles of air and the 5CB sample in the time domain. (c) THz transmission profile of 5CB in the frequency domain. The inset shows schematics of the THz transmission of 5CB LC in a vertical magnetic field. Absorption dips provide compelling evidence of THz light−phonon coupling in nematic mesogens.

Maxwell's relationship[53] ($\tau = \frac{\eta}{G_\infty}$, where G_∞ is the infinite-frequency shear modulus and η is the viscosity) we obtain the following relationship: $\omega = \frac{2\pi G_\infty}{\eta}$.[53−55] In solid materials, the viscosity is infinitely large compared with soft materials, and hence $\omega_{solid} = \frac{2\pi G_\infty}{\eta \to \infty} \to 0$. This means that the shear acoustic gap is absent and vibrational energy levels begin from the bottom of the potential well. However, in soft materials, η has a finite value and hence vibrational transverse energy levels begin from a nonzero value above the vibrational (phonon) gap. It should be pointed out that the acoustic phonon gaps can emerge in solid-based materials but only under certain conditions, for example, a restricted geometry.[56]

Scientific interest into the study of molecular sensitive vibrations in soft materials with nanoscale resolution is rapidly growing.[57−63] However, most experimental techniques are intrinsically unable to resolve the nanoscale molecular motions over any Q range. IXS is uniquely capable of determining the dynamic behavior of complex soft materials at the molecular level with ultrahigh energy-momentum resolution, something that is crucial for the development of future molecular sensitive nanotechnologies. Here, for the first time, we have provided compelling evidence of strong opto-acoustic phonon mixing in near-room-temperature nematic mesogens utilizing Q-resolved IXS, XRD, and THz TDS combined with atomistic MD simulations. A similar "waterfall" effect was previously observed in a ferroelectric perovskite system.[64] Specifically, an anomaly was discovered in the low-energy phonon dispersion due to interacting acoustic and soft optical branches. It is noteworthy that the mixing of longitudinal and transverse phonon polarizations in liquid water[65] and biological membranes[66] was also observed experimentally and from MD simulations, respectively. However, the detection of the opto-acoustic phonon mixing in a soft material (mesogens) was not previously reported, and may have far-reaching practical implications.

5CB LCs are both Raman- and THz light-active. This means that a portion of the energy can be pumped into the 5CB system by exposing it to THz light, which is then converted into nonpropagating, out-of-phase molecular motions (TO mode) due to light−phonon coupling. Furthermore, the nanoscale heat management can be realized via the control of propagating in-phase molecular vibrations (TA mode), which coexist with the TO mode. Because in-phase nanoscale rattling vibrations are sensitive to order-to-disorder,[36] the amount of transferred energy can be directly controlled by manipulating the acoustic phonon gap either by temperature or through an externally applied magnetic or electric field. Pioneered by Abbott et al.,[67] thermotropic LCs have recently been used as chemical and biological sensors, eliminating, in some cases, the need for fluorescent dyes.[68−75] A selective combination of LC

DOI: 10.1021/acs.jpclett.8b00926
J. Phys. Chem. Lett. 2018, 9, 2546−2553

sensitivity to external stimuli, combined with various opto-acoustic effects, may allow for the ultrafast visualization of dynamic responses, enabling the use of LCs for sensing applications. In this regard, nematic 5CB LCs are of fundamental importance for future nanoacoustic and opto-mechanical applications, utilizing key properties of mesogenic motions for sensing nanoscale rattling vibrations and THz light absorption.

AUTHOR INFORMATION

Corresponding Author

*E-mail: d.bolmatov@gmail.com, bolmatovd@ornl.gov.

ORCID

Dima Bolmatov: 0000-0003-4179-8971

Notes

The authors declare no competing financial interest.

ACKNOWLEDGMENTS

We thank Larry Carr, Alexey Suvorov, Yong Q. Cai, Mikhail Zhernenkov, Takeshi Egami, and Dmitry Bedrov for fruitful discussions. We acknowledge Xinzhong Chen for his assistance carrying out THz TDS measurements. The work at the National Synchrotron Light Source-II, Brookhaven National Laboratory, was supported by the U.S. Department of Energy, Office of Science, Office of Basic Energy Sciences under contract no. DE-SC0012704. We thank Alexey Suvorov, Yong Q. Cai, and Mikhail Zhernenkov for their assistance to carry out IXS measurements at 10-ID beamline, NSLS II. J.K. is supported through the Scientific User Facilities Division of the U.S. Department of Energy (DOE), Office of Basic Energy Sciences (BES), managed by UT-Battelle under contract no. DE-AC05 00OR2275.

REFERENCES

(1) Gray, G. W.; Harrison, K. J.; Nash, J. A. New family of nematic liquid crystals for displays. *Electron. Lett.* **1973**, *9* (6), 130−131.

(2) Goodby, J. W.; Waugh, M. A.; Stein, S. M.; Chin, E.; Pindak, R.; Patel, J. S. Characterization of a new helical smectic liquid crystal. *Nature* **1989**, *337*, 449−452.

(3) Goodby, J. W.; Waugh, M. A.; Stein, S. M.; Chin, E.; Pindak, R.; Patel, J. S. A new molecular ordering in helical liquid crystals. *J. Am. Chem. Soc.* **1989**, *111* (21), 8119−8125.

(4) Ihn, K. J.; Zasadzinski, J. A. N.; Pindak, R.; Slaney, A. J.; Goodby, J. Observations of the Liquid-Crystal Analog of the Abrikosov Phase. *Science* **1992**, *258*, 275−278.

(5) Acharya, B. R.; Primak, A.; Kumar, S. Biaxial Nematic Phase in Bent-Core Thermotropic Mesogens. *Phys. Rev. Lett.* **2004**, *92*, 145506.

(6) Lee, S.; Noda, K.; Hirata, S.; Vacha, M. Position-Dependent Three-Dimensional Diffusion in Nematic Liquid Crystal Monitored by Single-Particle Fluorescence Localization and Tracking. *J. Phys. Chem. Lett.* **2015**, *6* (8), 1403−1407.

(7) Schneider, J.; Zhang, W.; Srivastava, A. K.; Chigrinov, V. G.; Kwok, H. S.; Rogach, A. L. Photoinduced Micropattern Alignment of Semiconductor Nanorods with Polarized Emission in a Liquid Crystal Polymer Matrix. *Nano Lett.* **2017**, *17* (15), 3133−3138.

(8) Maldovan, M. Sound and heat revolutions in phononics. *Nature* **2013**, *503*, 209−217.

(9) Yang, L.; Zhang, Q.; Cui, Z.; Gerboth, M.; Zhao, Y.; Xu, T. T.; Walker, D. G.; Li, D. Ballistic Phonon Penetration Depth in Amorphous Silicon Dioxide. *Nano Lett.* **2017**, *17* (12), 7218−7225.

(10) Marronnier, A.; Lee, H.; Geffroy, B.; Even, J.; Bonnassieux, Y.; Roma, G. Structural Instabilities Related to Highly Anharmonic Phonons in Halide Perovskites. *J. Phys. Chem. Lett.* **2017**, *8* (12), 2659−2665.

(11) Ding, Z.; Zhou, J.; Song, B.; Chiloyan, V.; Li, M.; Liu, T. H.; Chen, G. Phonon Hydrodynamic Heat Conduction and Knudsen Minimum in Graphite. *Nano Lett.* **2018**, *18* (1), 638−649.

(12) Eichenfield, M.; Chan, J.; Camacho, R. M.; Vahala, K. J.; Painter, O. Optomechanical crystals. *Nature* **2009**, *462*, 78−82.

(13) Cummer, S. A.; Christensen, J.; Alu, A. Controlling sound with acoustic metamaterials. *Nat. Rev. Mater.* **2016**, *1*, 16001.

(14) Hur, K.; Hennig, R. G.; Wiesner, U. Exploring Periodic Bicontinuous Cubic Network Structures with Complete Phononic Bandgaps. *J. Phys. Chem. C* **2017**, *121* (40), 22347−22352.

(15) Schneider, D.; Liaqat, F.; El Boudouti, E. H.; El Hassouani, Y.; Djafari-Rouhani, B.; Tremel, W.; Butt, H.-J.; Fytas, G. Engineering the Hypersonic Phononic Band Gap of Hybrid Bragg Stacks. *Nano Lett.* **2012**, *12* (6), 3101−3108.

(16) Alonso-Redondo, E.; Schmitt, M.; Urbach, Z.; Hui, C. M.; Sainidou, R.; Rembert, P.; Matyjaszewski, K.; Bockstaller, M. R.; Fytas, G. A new class of tunable hypersonic phononic crystals based on polymer-tethered colloids. *Nat. Commun.* **2015**, *6*, 8309.

(17) Marino, A.; Arai, S.; Hou, Y.; Sinibaldi, E.; Pellegrino, M.; Chang, Y.-T.; Mazzolai, B.; Mattoli, V.; Suzuki, M.; Ciofani, G. Piezoelectric Nanoparticle-Assisted Wireless Neuronal Stimulation. *ACS Nano* **2015**, *9* (7), 7678−7689.

(18) Mork, A. J.; Lee, E. M. Y.; Dahod, N. S.; Willard, A. P.; Tisdale, W. A. Modulation of Low-Frequency Acoustic Vibrations in Semiconductor Nanocrystals through Choice of Surface Ligand. *J. Phys. Chem. Lett.* **2016**, *7* (20), 4213−4216.

(19) Wang, Y. M.; Judkewitz, B.; DiMarzio, C. A.; Yang, C. Deep-tissue focal fluorescence imaging with digitally time-reversed ultrasound-encoded light. *Nat. Commun.* **2012**, *3*, 928.

(20) Sato, A.; Pennec, Y.; Shingne, N.; Thurn-Albrecht, T.; Knoll, W.; Steinhart, M.; Djafari-Rouhani, B.; Fytas, G. Tuning and Switching the Hypersonic Phononic Properties of Elastic Impedance Contrast Nanocomposites. *ACS Nano* **2010**, *4* (6), 3471−3481.

(21) Wang, Q.; Yang, L.; Zhou, S.; Ye, X.; Wang, Z.; Zhu, W.; McCluskey, M. D.; Gu, Y. Phase-Defined van der Waals Schottky Junctions with Significantly Enhanced Thermoelectric Properties. *J. Phys. Chem. Lett.* **2017**, *8* (17), 2887−2894.

(22) George, J.; Shalabney, A.; Hutchison, J. A.; Genet, C.; Ebbesen, T. W. Liquid-Phase Vibrational Strong Coupling. *J. Phys. Chem. Lett.* **2015**, *6* (6), 1027−1031.

(23) Inagaki, M.; Motobayashi, K.; Ikeda, K. Electrochemical THz-SERS Observation of Thiol Monolayers on Au(111) and (100) Using Nanoparticle-assisted Gap-Mode Plasmon Excitation. *J. Phys. Chem. Lett.* **2017**, *8* (17), 4236−4240.

(24) Chen, I. J.; Mante, P. A.; Chang, C. K.; Yang, S. C.; Chen, H. Y.; Huang, Y. R.; Chen, L. C.; Chen, K. H.; Gusev, V.; Sun, C. K. Graphene-to-Substrate Energy Transfer through Out-of-Plane Longitudinal Acoustic Phonons. *Nano Lett.* **2014**, *14* (3), 1317−1323.

(25) Gelbwaser-Klimovsky, D.; Aspuru-Guzik, A. Strongly Coupled Quantum Heat Machines. *J. Phys. Chem. Lett.* **2015**, *6* (17), 3477−3482.

(26) Lee, H.; Ko, J. H.; Choi, J. S.; Hwang, J. H.; Kim, Y. H.; Salmeron, M.; Park, J. Y. Enhancement of Friction by Water Intercalated between Graphene and Mica. *J. Phys. Chem. Lett.* **2017**, *8* (15), 3482−3487.

(27) Hubener, H.; De Giovannini, U.; Rubio, A. Phonon Driven Floquet Matter. *Nano Lett.* **2018**, *18* (2), 1535−1542.

(28) Abe, K.; Hyeon-Deuk, K. Dynamical Ordering of Hydrogen Molecules Induced by Heat Flux. *J. Phys. Chem. Lett.* **2017**, *8* (15), 3595−3600.

(29) Shelton, D. J.; Brener, I.; Ginn, J. C.; Sinclair, M. B.; Peters, D. W.; Coffey, K. R.; Boreman, G. D. Strong Coupling between Nanoscale Metamaterials and Phonons. *Nano Lett.* **2011**, *11* (5), 2104−2108.

(30) Hsueh, C. C.; Gordon, R.; Rottler, J. Dewetting during Terahertz Vibrations of Nanoparticles. *Nano Lett.* **2018**, *18* (2), 773−777.

(31) Lee, J.; Lim, J.; Yang, P. Ballistic Phonon Transport in Holey Silicon. *Nano Lett.* **2015**, *15* (5), 3273−3279.

DOI: 10.1021/acs.jpclett.8b00926
J. Phys. Chem. Lett. 2018, 9, 2546−2553

(32) Bolmatov, D.; Zhernenkov, M.; Zav'yalov, D.; Stoupin, S.; Cai, Y. Q.; Cunsolo, A. Revealing the Mechanism of the Viscous-to-Elastic Crossover in Liquids. *J. Phys. Chem. Lett.* **2015**, *6*, 3048−3053.
(33) Kahl, P.; Baroni, P.; Noirez, L. Hidden solidlike properties in the isotropic phase of the 8CB liquid crystal. *Phys. Rev. E* **2013**, *88* (5), 050501.
(34) Bolmatov, D.; Zhernenkov, M.; Zav'yalov, D.; Cai, Y. Q.; Cunsolo, A. Terasonic Excitations in 2D Gold Nanoparticle Arrays in a Water Matrix as Revealed by Atomistic Simulations. *J. Phys. Chem. C* **2016**, *120* (35), 19896−19903.
(35) Zhernenkov, M.; Bolmatov, D.; Soloviov, D.; Zhernenkov, K.; Toperverg, B. P.; Cunsolo, A.; Bosak, A.; Cai, Y. Q. Revealing the mechanism of passive transport in lipid bilayers via phonon-mediated nanometre-scale density fluctuations. *Nat. Commun.* **2016**, *7*, 11575.
(36) Bolmatov, D.; Zhernenkov, M.; Sharpnack, L.; Agra-Kooijman, D. M.; Kumar, S.; Suvorov, A.; Pindak, R.; Cai, Y. Q.; Cunsolo, A. Emergent Optical Phononic Modes upon Nanoscale Mesogenic Phase Transitions. *Nano Lett.* **2017**, *17* (6), 3870−3876.
(37) Leadbetter, A.; Richardson, R.; Colling, C. The structure of a number of nematogens. *J. Phys. Colloq.* **1975**, *36*, 37−43.
(38) Cai, Y. Q.; Coburn, D. S.; Cunsolo, A.; Keister, J. W.; Honnicke, M. G.; Huang, X. R.; Kodituwakku, C. N.; Stetsko, Y.; Suvorov, A.; Hiraoka, N.; et al. The Ultrahigh Resolution IXS Beamline of NSLS-II: Recent Advances and Scientific Opportunities. *J. Phys.: Conf. Ser.* **2013**, *425*, 202001.
(39) Bolmatov, D.; Zhernenkov, M.; Zav'yalov, D.; Stoupin, S.; Cunsolo, A.; Cai, Y. Q. Thermally triggered phononic gaps in liquids at THz scale. *Sci. Rep.* **2016**, *6*, 19469.
(40) Bolmatov, D.; Musaev, E. T.; Trachenko, K. Symmetry Breaking Gives Rise to Energy Spectra of Three States of Matter. *Sci. Rep.* **2013**, *3*, 2794.
(41) Bolmatov, D.; Zav'yalov, D.; Zhernenkov, M.; Musaev, E. T.; Cai, Y. Q. Unified phonon-based approach to the thermodynamics of solid, liquid and gas states. *Ann. Phys.* **2015**, *363*, 221−242.
(42) Hsueh, H. C.; Vass, H.; Pu, F. N.; Clark, S. J.; Poon, W. C. K.; Crain, J. Low-frequency dynamics of liquid crystals. *Europhys. Lett.* **1997**, *38* (2), 107−112.
(43) Feller, S. E.; MacKerell, A. D. An Improved Empirical Potential Energy Function for Molecular Simulations of Phospholipids. *J. Phys. Chem. B* **2000**, *104* (31), 7510−7515.
(44) Tiberio, G.; Muccioli, L.; Berardi, R.; Zannoni, C. Towards in Silico Liquid Crystals. Realistic Transition Temperatures and Physical Properties for n-Cyanobiphenyls via Molecular Dynamics Simulations. *ChemPhysChem* **2009**, *10*, 125−136.
(45) Green, M. S. Markoff random processes and the statistical mechanics of time-dependent phenomena. II. Irreversible processes in fluids. *J. Chem. Phys.* **1954**, *22*, 398.
(46) Kubo, K. Statistical-mechanical theory of irreversible processes. I. General theory and simple applications to magnetic and conduction problems. *J. Phys. Soc. Jpn.* **1957**, *12*, 570.
(47) Wei, X.; Hooper, J. B.; Bedrov, D. Influence of electrostatic interactions on the properties of cyanobiphenyl liquid crystals predicted from atomistic molecular dynamics simulations. *Liq. Cryst.* **2016**, *44*, 332−347.
(48) Onsager, L. Reciprocal Relations in Irreversible Processes. I. *Phys. Rev.* **1931**, *37*, 405−426.
(49) Qiu, W.; Xi, L.; Wei, P.; Ke, X.; Yang, J.; Zhang, W. Part-crystalline part-liquid state and rattling-like thermal damping in materials with chemical-bond hierarchy. *Proc. Natl. Acad. Sci. U. S. A.* **2014**, *111* (42), 15031−15035.
(50) Ferguson, B.; Zhang, X. C. Materials for terahertz science and technology. *Nat. Mater.* **2002**, *1*, 26−33.
(51) Liu, M.; Hwang, H. Y.; Tao, H.; Strikwerda, A. C.; Fan, K.; Keiser, G. R.; Sternbach, A. J.; West, K. G.; Kittiwatanakul, S.; Lu, J.; et al. Terahertz-field-induced insulator-to-metal transition in vanadium dioxide metamaterial. *Nature* **2012**, *487*, 345−348.
(52) Vieweg, N.; Fischer, B. M.; Reuter, M.; Kula, P.; Dabrowski, R.; Celik, M. A.; Frenking, G.; Koch, M.; Jepsen, P. U. Ultrabroadband terahertz spectroscopy of a liquid crystal. *Opt. Express* **2012**, *20*, 28249−28256.
(53) Bolmatov, D.; Brazhkin, V. V.; Trachenko, K. The Phonon Theory of Liquid Thermodynamics. *Sci. Rep.* **2012**, *2*, 421.
(54) Heo, Y.; Bratescu, M. A.; Aburaya, D.; Saito, N. A phonon thermodynamics approach of gold nanofluids synthesized in solution plasma. *Appl. Phys. Lett.* **2014**, *104*, 111902.
(55) Iacobazzi, F.; Milanese, M.; Colangelo, G.; Lomascolo, M.; de-Risi, A. An explanation of the Al2O3 nanofluid thermal conductivity based on the phonon theory of liquid. *Energy* **2016**, *116*, 786−794.
(56) Sauceda, H. E.; Salazar, F.; Perez, L. A.; Garzon, I. L. Size and Shape Dependence of the Vibrational Spectrum and Low-Temperature Specific Heat of Au Nanoparticles. *J. Phys. Chem. C* **2013**, *117* (47), 25160−25168.
(57) Mattarelli, M.; Montagna, M.; Still, T.; Schneider, D.; Fytas, G. Vibration spectroscopy of weakly interacting mesoscopic colloids. *Soft Matter* **2012**, *8*, 4235−4243.
(58) Wang, P.; Rajian, J. R.; Cheng, J. X. Spectroscopic Imaging of Deep Tissue through Photoacoustic Detection of Molecular Vibration. *J. Phys. Chem. Lett.* **2013**, *4* (13), 2177−2185.
(59) Huix-Rotllant, M.; Ferre, N. An Effective Procedure for Analyzing Molecular Vibrations in Terms of Local Fragment Modes. *J. Chem. Theory Comput.* **2016**, *12* (10), 4768−4777.
(60) Cui, Y.; Lauchner, A.; Manjavacas, A.; García de Abajo, F. J. G.; Halas, N. J.; Nordlander, P. Molecular Plasmon-Phonon Coupling. *Nano Lett.* **2016**, *16* (10), 6390−6395.
(61) Dzierlenga, M. W.; Schwartz, S. D. Targeting a Rate-Promoting Vibration with an Allosteric Mediator in Lactate Dehydrogenase. *J. Phys. Chem. Lett.* **2016**, *7* (13), 2591−2596.
(62) Girard, A.; Gehan, H.; Crut, A.; Mermet, A.; Saviot, L.; Margueritat, J. Mechanical Coupling in Gold Nanoparticles Supermolecules Revealed by Plasmon-Enhanced Ultralow Frequency Raman Spectroscopy. *Nano Lett.* **2016**, *16* (6), 3843−3849.
(63) Holle, A. W.; Young, J. L.; Van Vliet, K. J.; Kamm, R. D.; Discher, D.; Janmey, P.; Spatz, J. P.; Saif, T. Cell-extracellular matrix mechanobiology: forceful tools and emerging needs for basic and translational research. *Nano Lett.* **2018**, *18* (1), 1−8.
(64) Hlinka, J.; Kamba, S.; Petzelt, J.; Kulda, J.; Randall, C. A.; Zhang, S. J. Origin of the "Waterfall" Effect in Phonon Dispersion of Relaxor Perovskites. *Phys. Rev. Lett.* **2003**, *91*, 107602.
(65) Sampoli, M.; Ruocco, G.; Sette, F. Mixing of Longitudinal and Transverse Dynamics in Liquid Water. *Phys. Rev. Lett.* **1997**, *79*, 1678.
(66) Conti Nibali, V. C.; D'Angelo, G.; Tarek, M. Molecular dynamics simulation of short-wavelength collective dynamics of phospholipid membranes. *Phys. Rev. E* **2014**, *89*, 050301.
(67) Gupta, V. K.; Skaife, J. J.; Dubrovsky, T. B.; Abbott, N. L. Optical Amplification of Ligand-Receptor Binding Using Liquid Crystals. *Science* **1998**, *279*, 2077−2080.
(68) Bi, X.; Hartono, D.; Yang, K. L. Real-Time Liquid Crystal pH Sensor for Monitoring Enzymatic Activities of Penicillinase. *Adv. Funct. Mater.* **2009**, *19*, 3760−3765.
(69) Bellini, T.; Zanchetta, G.; Fraccia, T. P.; Cerbino, R.; Tsai, E.; Smith, G. P.; Moran, M. J.; Walba, D. M.; Clark, N. A. Liquid crystal self-assembly of random-sequence DNA oligomers. *Proc. Natl. Acad. Sci. U. S. A.* **2012**, *109*, 1110−1115.
(70) Hunter, J. T.; Abbott, N. L. Adsorbate-Induced Anchoring Transitions of Liquid Crystals on Surfaces Presenting Metal Salts with Mixed Anions. *ACS Appl. Mater. Interfaces* **2014**, *6*, 2362−2369.
(71) Zhao, D.; Peng, Y.; Xu, L.; Zhou, W.; Wang, Q.; Guo, L. Nickel-Nanosphere-Induced Homeotropic Alignment for the Amplified Detection of Thrombin. *ACS Appl. Mater. Interfaces* **2015**, *7*, 23418−23422.
(72) Ohadi, D.; Uline, M. J. Molecular Modeling of Liquid Crystal/Phospholipid Interface as a Label-Free Biosensor. *Biophys. J.* **2017**, *112*, 592a.
(73) Liu, Q. Y.; Zuo, F.; Zhao, Z. G.; Chen, J.; Xu, D. Molecular dynamics investigations of an indicator displacement assay mechanism in a liquid crystal sensor. *Phys. Chem. Chem. Phys.* **2017**, *19*, 23924−23933.

DOI: 10.1021/acs.jpclett.8b00926
J. Phys. Chem. Lett. 2018, 9, 2546−2553

(74) Lee, H. G.; Munir, S.; Park, S. Y. Cholesteric Liquid Crystal Droplets for Biosensors. *ACS Appl. Mater. Interfaces* **2016**, *8* (39), 26407−26417.
(75) Popov, P.; Mann, E. K.; Jakli, A. Liquid-Crystal-Based Biosensor without Alignment Substrate. *Biophys. J.* **2014**, *106*, 415a.

NOTE ADDED AFTER ASAP PUBLICATION

This paper was published ASAP on May 2, 2018. An author name was corrected. The revised paper was reposted on May 9, 2018.

DOI: 10.1021/acs.jpclett.8b00926
J. Phys. Chem. Lett. 2018, 9, 2546−2553